Application of Remote Sensing and GIS to Estimate Evapotranspiration of Land Cover Types in Ba Ria-Vung Tau Province

Nhi Tuyet Thi Pham, Au Hai Nguyen*, Vo Nguyen Quang Khai, Vy Minh Hong Tat, Linh Khanh Luu, and Thien Duc Nguyen
Department of Geospatial Information Systems and Remote Sensing, The Institute for Environment and Resources, Vietnam National University, Ho Chi Minh City, Vietnam
Email: tuyetnhi.ier@gmail.com (N.T.T.P.); haiauvtn@gmail.com (A.H.N.); vonguyenquangkhai2654@gmail.com (V.N.Q.K.); tathongminhvy271@gmail.com (V.M.H.T.); luukhanhlinh1998@gmail.com (L.K.L.); thienduc295@gmail.com (T.D.N.)
*Corresponding author
Manuscript received May 13, 2025; revised July 1, 2025; accepted July 25, 2025; published December 17, 2025

***Abstract*—Evapotranspiration (ET) drives water loss from land surfaces, shapes regional hydrological balance, and fundamentally contributes to global sustainable resource management. Assessing ET is crucial for coastal areas heavily impacted by prolonged dry seasons, climate change, overexploitation of water resources, and pressures from urban development. This study employs remote sensing and Geographic Information Systems (GIS) to evaluate ET trends across Ba Ria-Vung Tau, a coastal province of Vietnam, from 2010 to 2020, using the Simplified Surface Energy Balance Index (S-SEBI) with Landsat imagery. The four land cover types analyzed were water, vegetation, bare soil, and impervious surfaces. The results showed that different land cover types in Ba Ria-Vung Tau province have revealed distinct ET patterns. Water surfaces exhibited the highest ET (15.01 ± 0.5 mm/day in 2020), followed by vegetation (6–10 mm/day), while bare soil and impervious surfaces ranged from 3–5 mm/day. In addition, land surface temperature (LST) emerged as a key factor directly influencing the amount of ET. LST rose from 27.8°C (2010) to 29.3°C (2020), raising ET by 7%, reflecting climate change and land use shifts. These findings show ET's key role in coastal water cycles and aid sustainable management amid urbanization and warming.**

***Keywords*—evapotranspiration, remote sensing, GIS, S-SEBI, Landsat, Ba Ria-Vung Tau**

I. Introduction

Evapotranspiration (ET) governs water flux from land to the atmosphere, influencing hydrological balance, agricultural productivity, and ecosystem stability [1]. In southern coastal regions like Ba Ria-Vung Tau Province, Vietnam, Estimating ET is critical for managing water resources under intensifying urbanization and climate change, particularly during dry seasons when water stress peaks [2, 3]. Traditionally, studies have relied on methods like lysimeters, which offer high accuracy but lack spatial scalability [4, 5]. In contrast, remote sensing—utilizing Landsat's 30 m resolution for Land Surface Temperature (LST) [6], Normalized Difference Vegetation Index (NDVI) [7], and albedo, enables cost-effective, large-scale analysis [8]. However, a key limitation of lysimeters is their inability to scale spatially despite their precision. While LST, NDVI, and albedo only provide indirect ET estimates. The Simplified Surface Energy Balance Index (S-SEBI) offers a practical compromise to address this. S-SEBI is an intermediate solution between accuracy and application scale, balancing accuracy and scalability for large-scale ET estimation, though it still requires calibration with field data.

Many approaches have been developed over the last few decades to estimate ET efficiently and accurately for various data conditions and regions. The most popular are meteorological models, of which the Penman–Monteith method recommended by Food and Agriculture Organization-FAO (FAO-56 PM) is considered the global standard due to its ability to integrate climatic and plant physiological factors [1]. However, this method requires complete meteorological data such as temperature, humidity, radiation, and wind speed. For regions with limited data, simpler empirical formulas such as Hargreaves–Samani [9] or Priestley–Taylor [10] are often used, although the accuracy may be lower if not properly calibrated. Physical hydrological models such as VIC (Variable Infiltration Capacity) are also applied to calculate ET on a basin or large regional scale, simulating evapotranspiration processes through the energy-water balance in the soil [11]. In addition, methods using remote sensing images such as SEBAL (Surface Energy Balance Algorithm for Land), METRIC (Mapping EvapoTranspiration at high Resolution with Internalized Calibration), S-SEBI, or TSEB (Thermal-Based Two-Source Energy Balance) are gradually receiving interest because of their ability to calculate ET over a large space, using data such as surface temperature (LST), NDVI index, albedo, and solar radiation from satellites [12]. These methods are especially useful in monitoring ET in areas that are difficult to access or lack monitoring stations. Experimental measurement methods such as lysimeters, eddy covariance, or pan evaporation provide real ET data with high accuracy; however, the implementation cost is high and is only applicable at some specific locations. In this study, the S-SEBI model - a simple and effective physical model based on the surface energy balance-was chosen because it fits Landsat image data well and does not require a lot of specific meteorological data.

On a regional scale, energy balance models like SEBAL [13, 14] and the Simplified Surface Energy Balance Index (S-SEBI) [15, 16] estimate ET with minimal ground data, unlike the data-intensive Penman-Monteith approach [1]. S-SEBI has proven simple and effective in tropical environments [17, 18], which reported Root Mean Squared Error (RMSE) values of 0.8–1.2 mm/day when comparing S-SEBI with SEBAL across diverse climates. Globally, ET varies significantly by land cover, with vegetated and water-rich areas exhibiting higher rates than urban zones [19]. Fisher *et al.* [20] estimated global ET at 65 ± 5 mm/month using thermal infrared data, highlighting

higher rates in humid tropics. In Thailand, Guan *et al.* [21] reported ET rates, solving the resolution difference between MODIS and Landsat data in tropical monsoon regions, underscoring the need for localized datasets. Additionally, Haiyang Shi [22] found that ET and temperature were weakly correlated in dry regions, while in humid regions the correlation was much higher, based on global data from 1700 to the present. In Vietnam, research on ET trends has utilized Landsat or MODIS (Moderate Resolution Imaging Spectroradiometer) satellite data in combination with the S-SEBI model to extract LST and land cover information and develop maps and models that illustrate these variations [23]. For example, Hung [23] highlighted the effectiveness of Landsat imagery in ET mapping in the northern coastal provinces of Vietnam. However, coastal Southeast Asia—where urbanization and warming disrupt water budgets—remains underexplored. Research shows that the S-SEBI model estimates the average daily actual ET (mm/day) in the Song Cau basin with an average absolute error of less than 20%. In Vietnam's southwest coastal region, Van Kich *et al.* [24] applied the SEBAL model with Sentinel-2 image for Soc Trang province, reporting ET rates ranging from 2 to 6 mm/day, depending on land cover and weather conditions, with 85–90% reliability compared to field data. However, the coastal provinces of the Southeast, specifically Ba Ria - Vung Tau and similar areas, have not been fully studied for their potential evapotranspiration, despite facing urbanization and climate-induced water stress.

Combining ET studies with the S-SEBI methodologically offers key advantages: minimizing the need for meteorological data, being effective with Landsat data, and being computationally faster than SEBAL or METRIC models. Accordingly, this study quantifies ET across Ba Ria-Vung Tau from 2010 to 2020 using S-SEBI, providing the first spatiotemporal ET dataset for a Vietnamese coastal province to inform sustainable water management amid these pressures. An accurate, detailed ET database enhances water resources management, environmental protection, and sustainable development for global coastal areas.

This study estimated evapotranspiration (ET) trends across Ba Ria–Vung Tau Province during 2010–2020 using the S-SEBI model and Landsat imagery. The results show that water bodies, forests, and vegetated areas exhibited significantly higher ET values compared to bare land and impervious surfaces. Moreover, rising Land Surface Temperature (LST) was found to correlate with increased ET, reflecting the combined impacts of climate change and land use change on the region.

II. Materials and Methods

A. Study Area

Ba Ria-Vung Tau Province, located in southeastern Vietnam (107°00′01″–107°34′18″E, 10°19′08″–10°48′39″N), covers 1982.56 km², excluding Con Dao District [25] (Fig. 1). The landscape gradually descends from the northeast toward the south and southwest, featuring elevated mountain ranges in the east and southeast with altitudes ranging from 118 to 500 meters. In contrast, the western area along the Thi Vai River consists of low-lying coastal marshes that have evolved into mangrove ecosystems. The topography of Ba Ria-Vung Tau can be categorized into four distinct zones: the peninsula, the hilly and semi-mountainous region, the coastal plains and valleys, and the marine and island zone. Bordering the East Sea, it experiences a tropical monsoon climate with a rainy season (May–October) and a dry season (November–April). It has an average annual temperature of 27°C, approximately 2400 sunshine hours, and 1500 mm of rainfall. According to the General Statistics Office [26], temperatures increase noticeably from March to July, ranging from 28°C to 29.3°C. Sunshine hours peak in the first six months at around 260 hours per month, dropping to about 160 hours per month for the remainder of the year. Monthly rainfall varies significantly: the first two months (January–February) see almost no rain, and the next four (March–June) and last two (November–December) average light rainfall of approximately 100 mm/month. Meanwhile, July to October brings heavy rainfall, peaking at 245–360 mm/month. Its coastal location and minimal typhoon activity underscore its susceptibility.

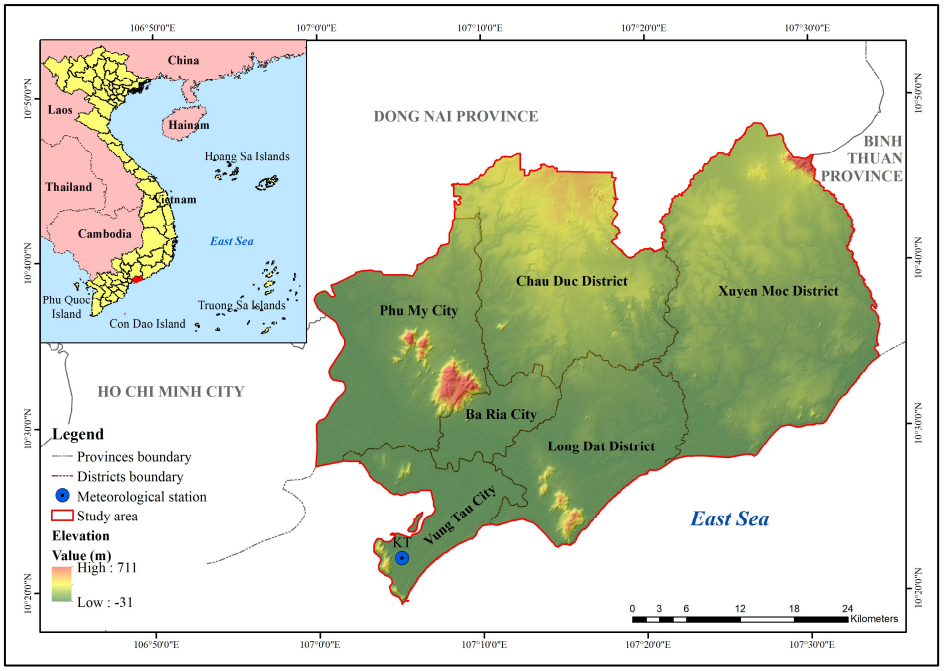

Fig. 1. Location map of Ba Ria-Vung Tau province, Vietnam.

B. Data

This study utilized remote sensing data from Landsat 5 and Landsat 8 satellite imagery, alongside 30 m SRTM (Shuttle Radar Topography Mission) Digital Elevation Models (DEMs) sourced from the United States Geological Survey (USGS) Earth Explorer platform: https://earthexplorer.usgs.gov. Landsat 5 imagery, captured on February 4, 2010, using the Thematic Mapper (TM) sensor with a 30 × 30 m resolution, and Landsat 8 imagery, acquired on January 17, 2015, and January 15, 2020, using the Operational Land Imager and Thermal Infrared Sensor (OLI_TIRS) and a resolution of 30 × 30. Landsat 5 imagery was preferred over Landsat 7 to avoid striping errors caused by the latter's Scan Line Corrector failure for more complete and accurate image reconstruction. Image selection prioritized cloud-free conditions (<10% cloud cover) in the study area and temporal consistency within the dry season, with acquisition dates aligned accordingly. Acquisition dates minimized cloud cover (<10%) and aligned with dry season consistency (Table 1). Cloud cover during the rainy season posed a potential limitation, though it was mitigated by careful date selection.

Table 1. Satellite imagery details

No.	Source	Date	Resolution (m)	Cloud cover (%)
1	Landsat 5-LT51240532010035BKT00	Feb 4, 2010	30	6.0
2	Landsat 8-LC81240532015017LGN01	Jan 17, 2015	30	7.47
3	Landsat 8-LC81240532020015LGN00	Jan 15, 2020	30	0.41
4	SRTM DEM	Sep 23, 2014	30	

Table 2. NASA power meteorological data at Vung Tau

Year	Solar Radiation (MJ/m²/day)	Air Temperature (°C)	Relative Humidity (%)	Surface Pressure (kPa)	Wind Speed at 2m (m/s)
2010	23.38	26.18	75.85	101.04	4.17
2015	20.12	25.37	67.86	101.15	2.86
2020	21.59	26.73	64.87	100.99	3.93

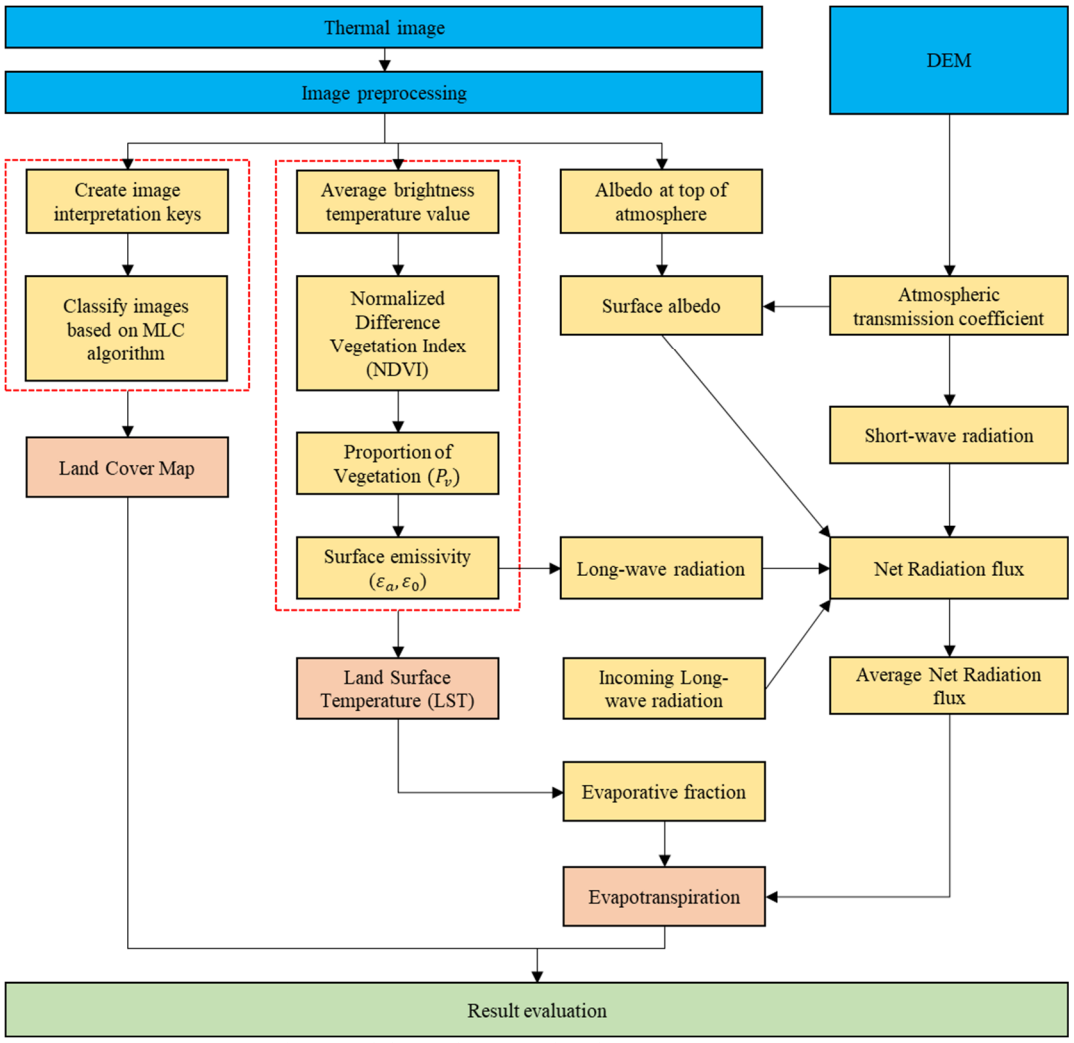

Fig. 2. Workflow of the S-SEBI-based ET estimation process.

Meteorological data for the study area were sourced from the reanalysis dataset NASA POWER (Prediction of Worldwide Energy Resources) project, accessed through the NASA POWER web portal (https://power.larc.nasa.gov/) because ground-based meteorological observations from the Vung Tau station were not accessible for this study due to

data availability constraints and permission restrictions. The data were retrieved for the grid cell corresponding to the Vung Tau meteorological station (10.34°N, 107.08°E) in Ba Ria-Vung Tau Province, Vietnam. Atmospheric variables (e.g., temperature, humidity, wind speed, solar radiation, and surface pressure) were retrieved for the years 2010, 2015, and 2020 to calculate potential Evapotranspiration (ETp) using the FAO-56 Penman-Monteith method. These years were selected to correspond with the acquisition dates of satellite imagery used in this study, ensuring temporal alignment between meteorological conditions and remote sensing data for integrated analysis. Several studies have successfully validated the use of NASA POWER data for evapotranspiration assessment and environmental applications across diverse climatic regions [27, 28]. Therefore, in this study, the ETp derived from NASA POWER data was used as a reference to evaluate the accuracy of the evapotranspiration estimated by the S-SEBI model. The comparison serves to validate the S-SEBI results under local climatic conditions, supporting the applicability of remote sensing approaches in areas with limited ground-based measurements (Fig. 2).

Administrative boundary data for Vietnam, updated as of July 19, 2022, were obtained from the DIVA-GIS website: https://www.diva-gis.org. The data includes Vietnam's administrative boundary map used in Shapefile (*shp) format and is classified into three levels: provincial, district, and commune. Details of the Landsat satellite imagery, DEM data, and NASA POWER used in this study are presented in Tables 1–2.

C. Methods

This study estimates ET using the Simplified Surface Energy Balance Index (S-SEBI) model, which leverages Landsat imagery to balance accuracy with minimum ground data requirements [21], which is ideal for the sparse meteorological network of Ba Ria - Vung Tau. The method includes image preprocessing, land cover classification, LST inference, ET estimation, and validation (Fig. 2).

1) Image preprocessing

Before image analysis, preprocessing is essential to correct for atmospheric conditions. Converting image channels to Surface Reflectance (SR) ensures practical utility [2]. After the acquisition, satellite images of Landsat 5 (2010) and Landsat 8 (2015, 2020) were corrected by digital radiation measurement (DN) into spectral reflectance values. Correction formulas vary by Landsat sensor type. The DN-to-Top-of-Atmosphere (TOA) reflectance model is commonly applied due to the absence of a universal correction model for all regions [29]. In practice, TOA reflectance is often used as an approximation of SR reflectance despite their differences due to computational complexity. Following USGS protocols, Landsat imagery in this study was corrected from DN to TOA reflectance, minimizing atmospheric interference. Cloud-free images (<10% cloud cover) were selected during the dry season (January–February) to ensure temporal consistency (Table 1).

2) Land cover classification

Following geometric preprocessing, this study utilized sample points collected during fieldwork in Ba Ria-Vung Tau province to establish land cover maps and assess classification accuracy. After developing the interpretation key, the 'ROI Tool' in ENVI software was used to define training samples for classifying land cover across two periods (2010 and 2020). Supervised classification via Maximum Likelihood Classifier identified four land cover types-water, vegetation, bare soil, and impervious surfaces-using field-collected training samples (n = 50 per class) in 2024.

Training sample separability was assessed using discriminant values to evaluate classification reliability, as outlined in Refs. [30, 31]; values exceeding 1.9 indicate good separation. The discriminant values in this study (1.806–2.0) suggest sufficient reliability for distinguishing land cover types in satellite imagery. In addition to the overall accuracy, the Kappa coefficient (K) was also calculated to assess the agreement between the classified map and the reference data, accounting for chance agreement. The Kappa coefficient (Eq. (1)) is widely used in remote sensing accuracy assessment and was originally introduced by Cohen (1960):

$$K = \frac{p_0 - p_e}{1 - p_e} \quad (1)$$

where: p_0 is the observed agreement. p_e is the expected agreement by chance, based on the row and column totals of the confusion matrix.

3) Surface temperature

LST is an important parameter in the physical processes of different surfaces at multiple scales. LST is derived from the thermal bands using brightness temperature, NDVI, vegetation fraction, and emissivity (according to Eqs. (2–4)) [32]. Convert the TOA (Top of Atmosphere) radiation value to TOA brightness temperature value using the formula below with the temperature constant provided in the Landsat image metadata file for band 10 of Landsat 8 image, K_1 = 774.8853; K_2 = 1321.0789. LST was derived from thermal bands using brightness temperature (Tb T_b Tb), NDVI, vegetation fraction (Pv P_v Pv), and emissivity (ε \varepsilon ε) equations [32]:

$$T_b = \frac{K_2}{\ln\left(\frac{K_1}{L_\lambda} + 1\right)} - 273.15 \quad (2)$$

where: K_1 & K_2: thermal conversion constant, and it varies for both TIR bands. L_λ: Top of Atmospheric spectral radiance. The value of L_λ was obtained from the metadata files accompanying the Landsat Level-1 data products, as provided by the U.S. Geological Survey (USGS) via https://www.usgs.gov/landsat-missions/using-usgs-landsat-level-1-data-product.

NDVI is a standard algorithm designed to estimate the quality of green vegetation on the ground using reflectance measurements at red and near-infrared wavelengths [32]:

$$\text{NDVI} = \frac{NIR - RED}{NIR + RED} \quad (3)$$

where: NIR: Near-Infrared reflectance of Landsat. RED: Red Band reflectance of Landsat.

The NDVI index measures the greenness of vegetation and is used to calculate the vegetation cover ratio (Pv), surface emissivity (ε), and radiant energy levels. Its outstanding advantages are that it is easy to calculate, widely available,

and compatible with Landsat images in low-noise environments such as cloud cover or complicated terrain. Therefore, the selection of NDVI is an important part to ensure continuity throughout the entire input data processing chain for the S-SEBI model. In recent studies such as Afzal *et al.* (2021) and Singh *et al.* (2021) [33, 34], NDVI continues to be widely used due to its easy integration into surface energy models, the most popular and simple for agricultural drought monitoring, and used as a basic index for assessing greenness and monitoring long-term vegetation changes. However, the study also noted the limitations of this index, such as its susceptibility to saturation in dense vegetation areas, its dependence on ground and lighting conditions, and its dependence on sun angle, terrain, clouds, and fog, and suggested that in future studies, it be compared to improved indexes such as EVI (Enhanced Vegetation Index) or SAVI (Soil Adjusted Vegetation Index) to improve accuracy in complex terrain conditions.

LST (T_s) is the radiant temperature calculated using the luminous temperature, the wavelength of emitted radiation used for surface temperature calculation corresponds to the effective center wavelength of the thermal bands from the respective Landsat sensors which was set to 11.45 μm for Landsat 5 TM and 10.8 μm for Landsat 8 OLI/TIRS according to USGS Landsat product specifications https://www.usgs.gov/landsat-missions, and land surface emissivity.

$$T_s = \frac{T_b}{1 + \left(\lambda \frac{T_b}{\rho}\right) Ln(\varepsilon)} \quad (4)$$

where: T_b: Brightness temperature (°C). λ: Wavelength of Emitted Radiance (μm). ρ: Boltzmann/Planck's constant. ε: Surface emissivity.

4) S-SEBI model

The S-SEBI model calculates ET as a function of net radiation (R_n), evaporation fraction (ETF) and daily latent heat flux (according to Eqs. (5–7)) [18], selected for its efficacy with single-date satellite imagery and minimal ground data requirements, and its effectiveness in data-scarce tropical locations such as Ba Ria-Vung Tau [28] instead of advanced machine learning methods that require large data sources.

$$R_n = (1 - \alpha)R_S \downarrow + R_L \downarrow - R_L \uparrow \quad (5)$$

where: R_n: Net Radiation flux (W/m^2). α: Surface Albedo. R_S: Incoming shortwave radiation (W/m^2). R_L: Incoming longwave radiation (W/m^2). $R_L \uparrow$: Outgoing longwave radiation (W/m^2).

$$ETF_i = \frac{T_{s,dry} - T_s}{T_{s,dry} - T_{s,wet}} \quad (6)$$

where: ETF_i: Evaporative Fraction. T_s: Surface Temperature (°C). $T_{s,wet}$, where $s, wet_{\max}(r_o) = R\text{-}G_o$ and $s, dry = 0$ and a reflectance dependant temperature, $T_{s,dry}$, where, $s, dry_{\max}(r_o) = R\text{-}G_o$ and $s, wet = 0$.

$$ET_a = ETF_i . \frac{R_{n,d}}{\lambda} \quad (7)$$

where: ET_a: Evapotranspiration (mm). ETF_i: Evaporative Fraction. $R_{n,d}$: Daily net radiation flux (MJ/m^2/day).

λ: The daily evaporation heat quantity is 2.45 MJ/Kg [17].

5) Validation

The potential Evapotranspiration (ETp) was calculated using the FAO-56 Penman–Monteith equation by using NASA POWER data at Vung Tau station, which combines radiative and aerodynamic components to estimate ET under standard reference conditions. The equation is expressed as follows [1] Eq. (8):

$$ET_p = \frac{0.408\Delta(R_n - G) + \gamma \frac{900}{T + 273} u_2 (e_s - e_a)}{\Delta + \gamma(1 + 0.34u_2)} \quad (8)$$

where: ET_p is the potential evapotranspiration (mm/day). R_n is the net radiation (MJ/m²/day). G is the soil heat flux density (MJ/m²/day). T is the mean daily air temperature (°C). u_2 is the wind speed at 2 m height (m/s). e_s is the saturation vapor pressure (kPa). e_a is the actual vapor pressure (kPa). Δ is the slope of the saturation vapor pressure curve (kPa/°C). γ is the psychrometric constant (kPa/°C).

ET estimates were validated against data from three meteorological stations within the province, using correlation coefficients, Mean Squared Error (MSE), and Root Mean Squared Error (RMSE) (Eq. (9)) [35], calculated as:

$$RMSE = \sqrt{\frac{1}{n}\sum_{i=1}^{n} \left(ET_{model,i} - ET_{observed,i}\right)^2} \quad (9)$$

where: n: number of data points. $ET_{model,i}$: Estimated evapotranspiration value from the model at point i. $ET_{observed,i}$: Observed evapotranspiration value at point i.

In addition to evaluating model performance through spatial comparison and visual analysis, potential Evapotranspiration (ETp) values calculated using the FAO-56 Penman-Monteith method from NASA POWER reanalysis data were used as reference points at the Vung Tau station location. These values were compared with the corresponding ETa results extracted from the S-SEBI model at the same location and acquisition dates. The Root Mean Square Error (RMSE) between ETa and ETp across the years 2010, 2015, and 2020 was calculated to quantify the model's accuracy under local climatic conditions. This approach enhances the reliability of the S-SEBI estimation in regions lacking in-situ measurements.

III. Results

A. Land Cover Dynamics

Due to the lack of historical field data, the study conducted a field survey in March 2024 to collect representative sample points for the main land cover types: water surface, vegetation, bare soil, and impervious surface. To reduce mistakes, the study used Google Earth images to choose extremely stable items for training and validation data, including water surfaces, impermeable surfaces, perennial plants, and persistent bare soil. The classification results were then overlaid with ET to estimate the area of land cover types and their ET.

Intermediate calculated values such as Surface emissivity; Brightness temperature; Net radiation flux; Evaporative fraction were calculated from Landsat 5 and Landsat 8 images, using the Raster Calculator tool of ArcMap software (shown in Figs. A1–A2 in the Appendix).

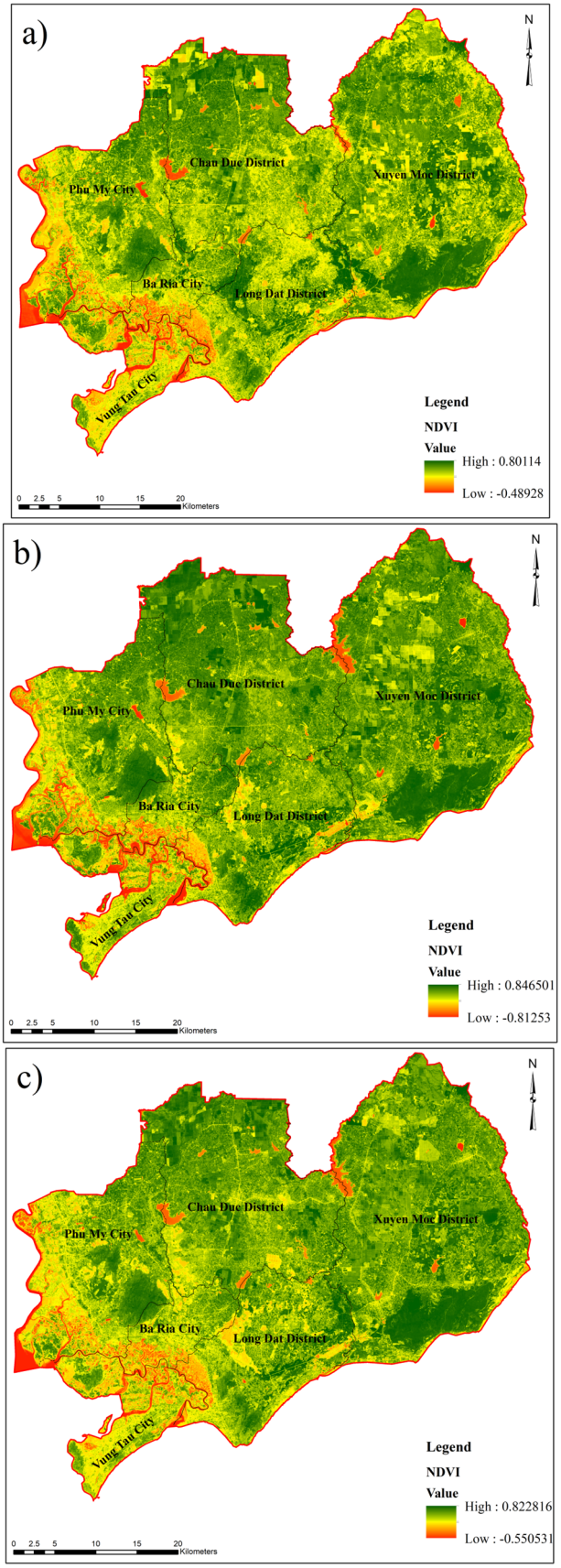

Fig. 3. Normalized difference vegetation index (NDVI) for (a) 2010, (b) 2015, and (c) 2020.

NDVI values calculated from Landsat images in the dry seasons of 2010, 2015, and 2020 ranged from −0.81 to 0.85 (Fig. 3). Low NDVI values are mainly located in hydrological objects, including the Thi Vai River, Dinh River, Ray River, river systems, small streams, and lakes in Ba Ria-Vung Tau province. Areas with low to medium NDVI values are typically seen in residential areas, construction sites, and bare land. Forested and green areas are places with medium to high NDVI values, which clearly reflect the difference between types of land cover. The NDVI peaked in 2015 (0.846), higher than in 2010 (0.801) and 2020 (0.822), indicating that greening levels may have been higher in 2015, possibly related to favorable climatic conditions or increased cropped area, and representing a slight change in greening levels over time.

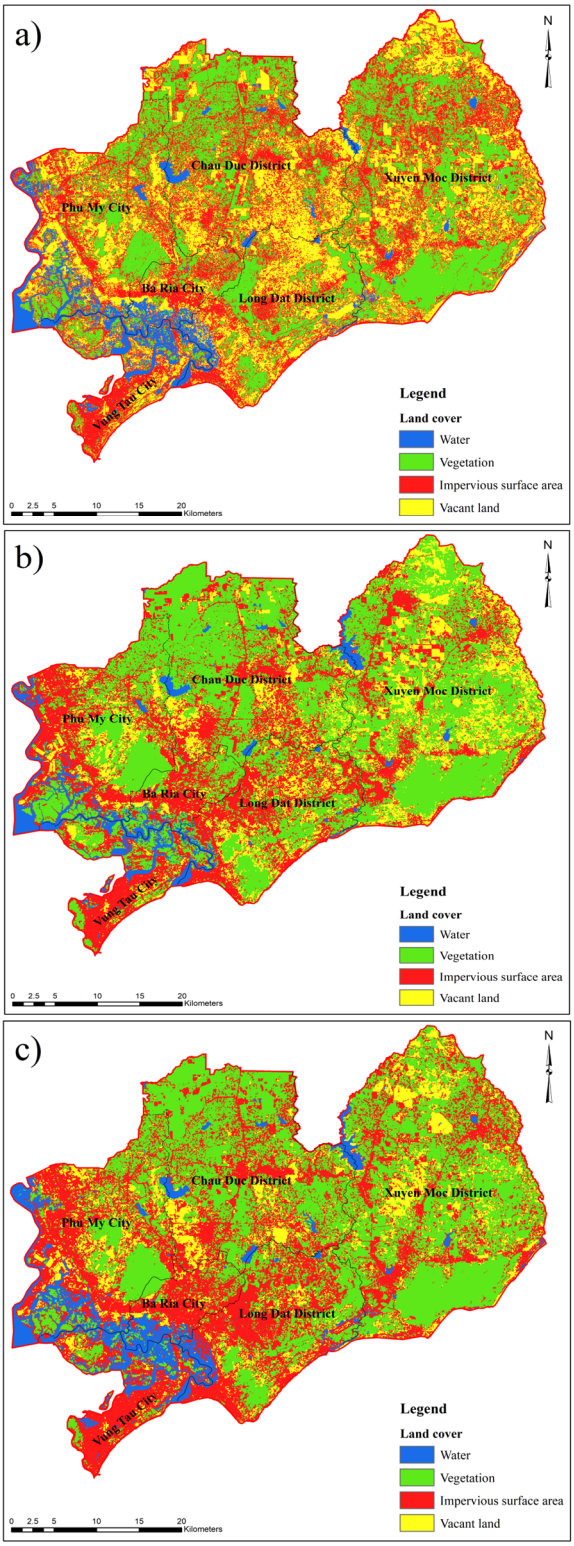

Fig. 4. Land cover maps for (a) 2010, (b) 2015, and (c) 2020, illustrating the spatial distribution of water (blue), vegetation (green), vacant soil (yellow), and impervious surfaces (red).

Impervious surfaces expanded from 678.68 km² (35.59%) in 2010 to 725.63 km² (38.06%) in 2020, while bare soil declined from 511.77 km² (26.84%) to 224.14 km² (11.76%), reflecting urbanization (Table 3) (Fig. 4). Classification accuracy exceeded 70%, with Kappa coefficients >0.6 (Table 4), comparable to [23, 36].

Table 3. Land cover area and percentage (2010–2020)

Year	Land Cover Type	Area (km²)	Percentage (%)
2010	Water	111.88	5.87
	Vegetation	604.51	31.70
	Impervious Surfaces	678.68	35.59
	Vacant Soil	511.77	26.84
2015	Water	91.33	4.79
	Vegetation	897.74	47.09
	Impervious Surfaces	615.51	32.29
	Vacant Soil	301.81	15.83
2020	Water	131.89	6.92
	Vegetation	824.67	43.26
	Impervious Surfaces	725.63	38.06
	Vacant Soil	224.14	11.76

Table 4. Classification accuracy metrics

Metric	2010	2015	2020
Overall Accuracy (%)	76.71	80.82	82.19
Kappa Coefficient	0.687	0.742	0.761

Classification accuracy and Kappa coefficients for 2010, 2015, and 2020 were consistently high. In 2010, overall accuracy reached 76.71%, with a Kappa coefficient of 0.6870. Some errors occurred because field data were collected in March 2024, long after 2010, when land cover and land use changes likely introduced discrepancies. By 2015, overall accuracy improved to 80.82%, and the Kappa coefficient rose to 0.7419, reflecting better agreement between the classification results and the reference data. In 2020, overall accuracy increased to 82.19%, with a Kappa of 0.7607. This trend suggests progressively higher accuracy over time, possibly due to minimal land cover changes between 2020 and the 2024 sampling period. Enhancing the consistency between field data and 2020 satellite imagery. These reliable results, supported by high accuracy and robust classification, justify their use in further studies and enable the development and refinement of land cover maps for Ba Ria-Vung Tau Province.

B. LST and ET Variations

1) LST results

LST increased from 27.8°C in 2010 to 29.3°C in 2020, driving ET from 4–8 mm/day to 6–15 mm/day. Water surfaces recorded the highest ET, peaking at 15.01 ± 0.5 mm/day in 2020, surpassing the 12 mm/day reported for the Cau River Basin [23], likely due to elevated coastal humidity. Vegetation exhibited ET rates of 6–10 mm/day, while bare soil and impervious surfaces ranged from 3–5 mm/day (Tables 5–7). The 7% ET rise aligns with regional warming trends.

Table 5. Land surface temperature and Evapotranspiration by land cover for 2010

Land Cover Type	LST Min (°C)	LST Max (°C)	ET (mm/day) ± SD
Water	22.82	31.25	8.46 ± 0.4
Vegetation	21.07	32.47	6.47 ± 0.3
Impervious Surfaces	18.84	35.27	4.98 ± 0.2
Vacant Soil	22.82	35.66	4.03 ± 0.2

Table 6. Land surface temperature and Evapotranspiration by land cover for 2015

Land Cover Type	LST Min (°C)	LST Max (°C)	ET (mm/day) ± SD
Water	21.03	26.09	13.45 ± 0.5
Vegetation	19.66	31.14	7.78 ± 0.4
Impervious Surfaces	19.14	37.05	5.00 ± 0.3
Vacant Soil	21.19	38.89	2.92 ± 0.2

Table 7. Land surface temperature and Evapotranspiration by land cover for 2020

Land Cover Type	LST Min (°C)	LST Max (°C)	ET (mm/day)±SD
Water	23.68	31.16	15.01 ± 0.5
Vegetation	23.37	34.79	10.80 ± 0.4
Impervious Surfaces	22.03	41.74	8.95 ± 0.3
Vacant Soil	24.50	45.85	6.76 ± 0.3

LST calculations reveal distinct shifts over time. In 2010, temperatures predominantly ranged from 22°C to 31°C, with most areas between 25°C and 31°C. Areas with higher temperatures (from 31°C to above 34°C) were quite limited, appearing only sporadically in certain areas. By 2015, LST increased, with areas from 28°C to >34°C expanding compared to 2010. Moreover, regions exceeding 34°C, growing notably in the central and northern parts of the province. In 2020, LST continued to rise and spread, with temperatures from 28°C to >34°C dominating most of the area. Compared to 2015, areas above 34°C expanded significantly, particularly in the south and east. Possibly linked to increased impervious surfaces from urbanization or reduced green cover (Figs. 5–6).

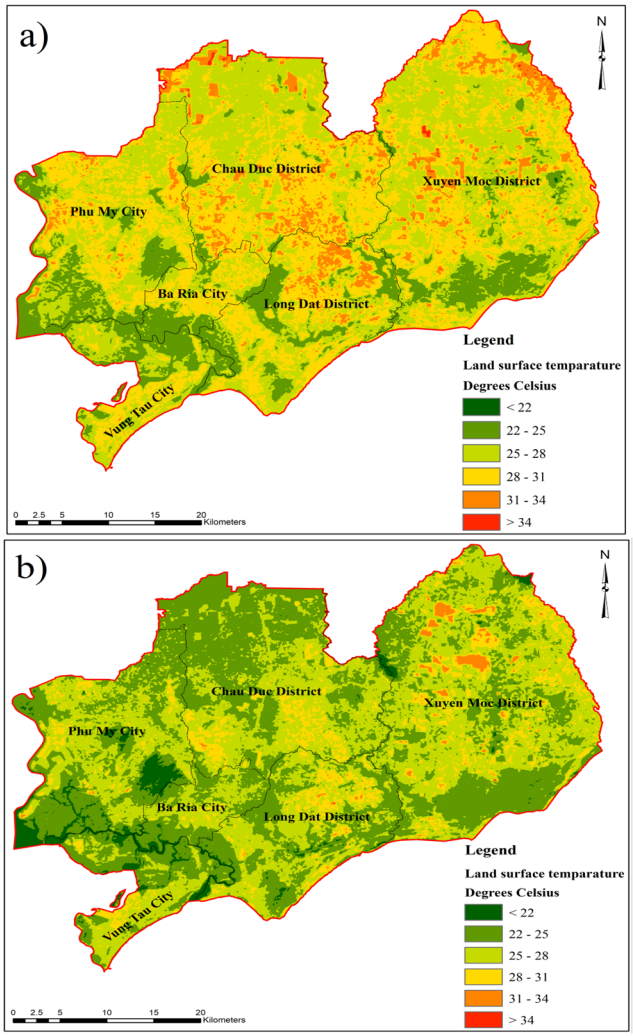

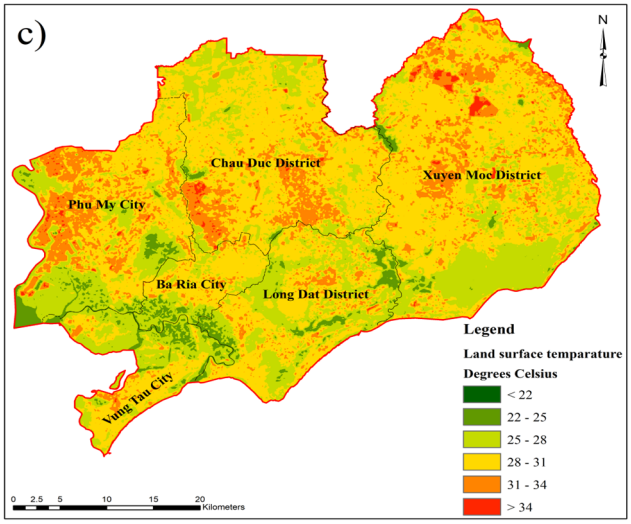

Fig. 5. Land surface temperature maps for (a) 2010, (b) 2015, and (c) 2020.

2) ET results

To calculate ET, the regressor variables (Table 8) extracted from the graph (Fig. 6) characterize the surface temperature and albedo, which are used for the calculations in Eqs. (6–7).

In 2010, calculated ET values predominantly ranged from 4 to 8 mm/day, with areas of high ET (>8 mm/day) being relatively limited. By 2015, ET increased significantly, with values spanning 6–9 mm/day and some areas reaching 9–12 mm/day. High-ET areas expanded compared to 2010, particularly in the northern and central parts of the province. Reflecting a broader distribution of average and elevated ET indicates changes in land cover or weather conditions. This upward trend continued in 2020, with high-ET areas (>15 mm/day) becoming prominent in the northern and central regions. Compared to 2010 and 2015, these areas expanded substantially, suggesting influences from rising temperatures or shifts in land use and land cover.

However, it is important to note that these results represent ETa on single days during the dry season (February 4, 2010; January 17, 2015; and January 15, 2020). ETa can fluctuate significantly on a daily basis due to meteorological changes; thus, single-date comparisons primarily reflect spatial distribution and model consistency rather than annual ETa trends. To address this limitation, potential Evapotranspiration (ETp) was also calculated using NASA POWER meteorological data on the same days via the FAO-56 Penman–Monteith method. These values serve as a benchmark to evaluate the accuracy of the S-SEBI-derived ETa.

Table 8. Albedo and surface temperature relationship over the years

		2010	2015	2020
TH	a	35,748	3357	36,815
	b	−16,727	−14,071	−15,878
TLE	a	21,786	19,387	22,187
	b	16,428	16,443	19,082

a)

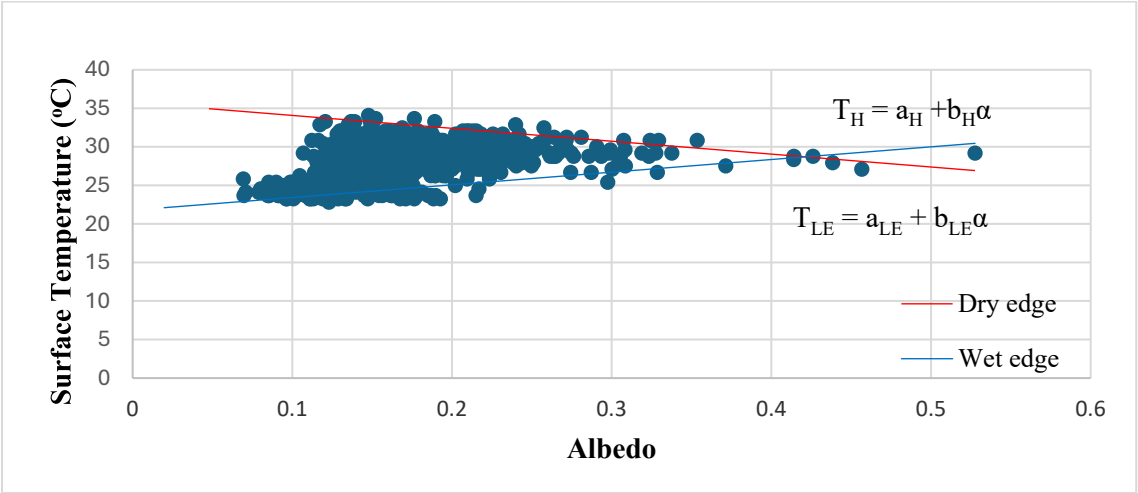

b)

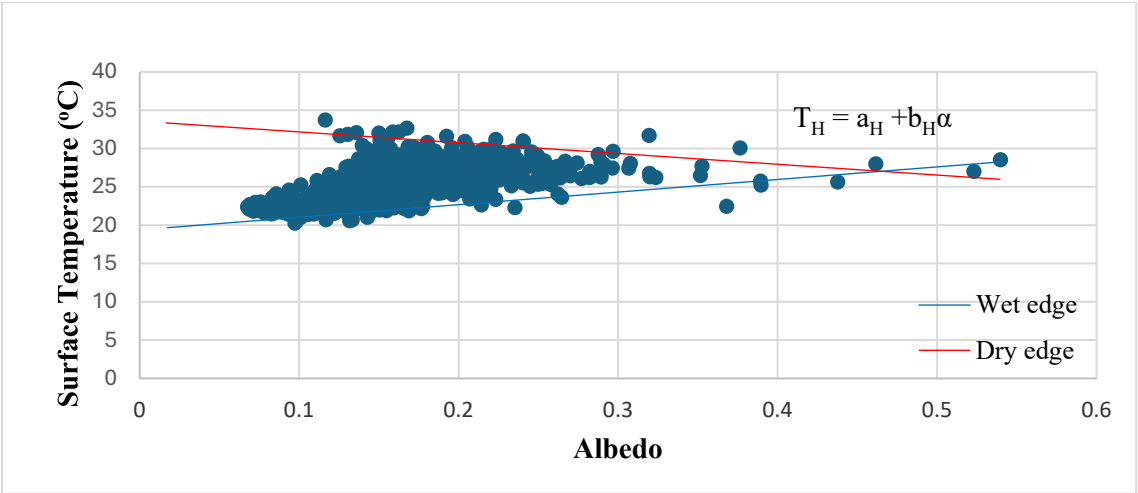

c)

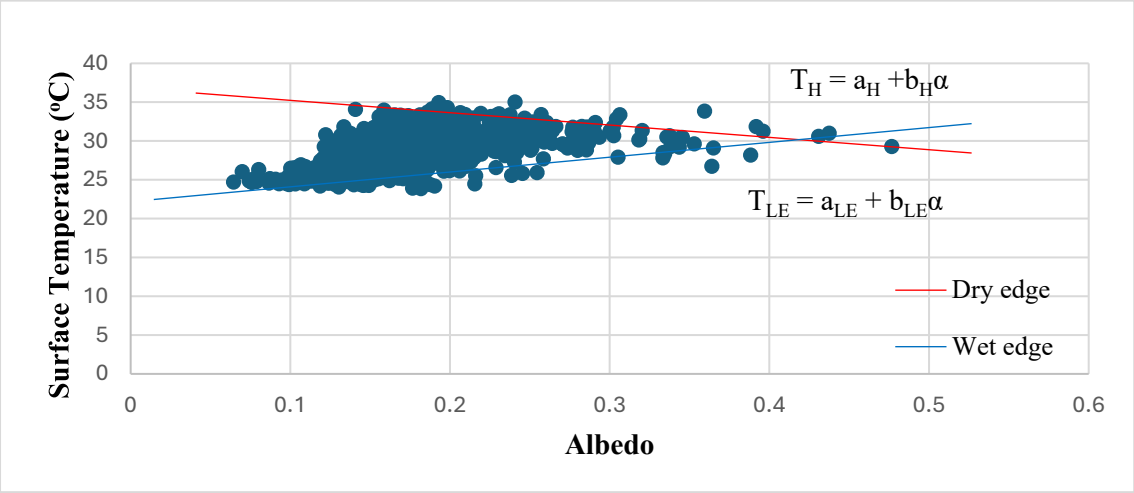

Fig. 6. Albedo and surface temperature in (a) 2010, (b) 2015, and (c) 2020.

Table 9. Comparison of S-SEBI estimated ETa and FAO-56 ETp (NASA POWER) at Vung Tau station (2010–2020)

Year	ETa (S-SEBI) (mm/day)	ETp (FAO56, NASA POWER) (mm/day)	Difference (ETa − ETp)
2010	4.31	7.4	−3.09
2015	8.8	6.86	+1.94
2020	7.26	7.84	−0.58

Table 9 presents the comparison between actual Evapotranspiration (ETa) estimated by the S-SEBI model and potential Evapotranspiration (ETp) calculated using the FAO-56 Penman–Monteith method with NASA POWER data at the Vung Tau station location. The results show variation between ETa and ETp across the three years, with an overall RMSE of 2.13 mm/day. Notably, the highest ETa values (e.g., 15.01 mm/day in 2020 for water surfaces) were not uniform across the study area but occurred at scattered pixels with specific surface and temperature conditions, consistent with localized thermal and radiative processes. These high values are therefore not indicative of average ET across water bodies.

After classifying land cover types, their impacts on Land Surface Temperature (LST) and Evapotranspiration (ET) in Ba Ria-Vung Tau Province were analyzed by integrating LST and ET data Ba Ria-Vung Tau Province were analyzed. ArcMap software tools generated a diagram illustrating the relationship between surface temperature, ET, and land cover types (Figs. 7–8).

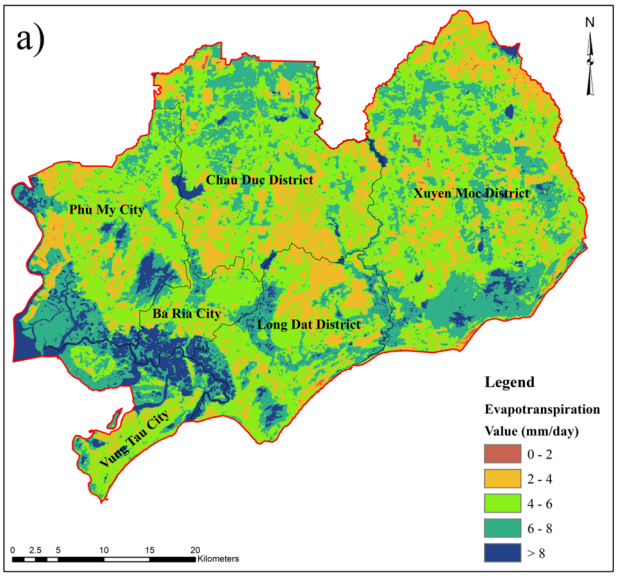

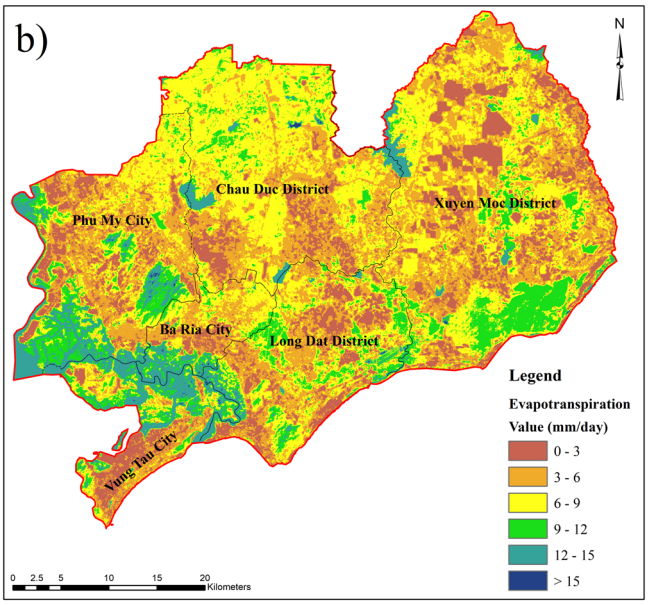

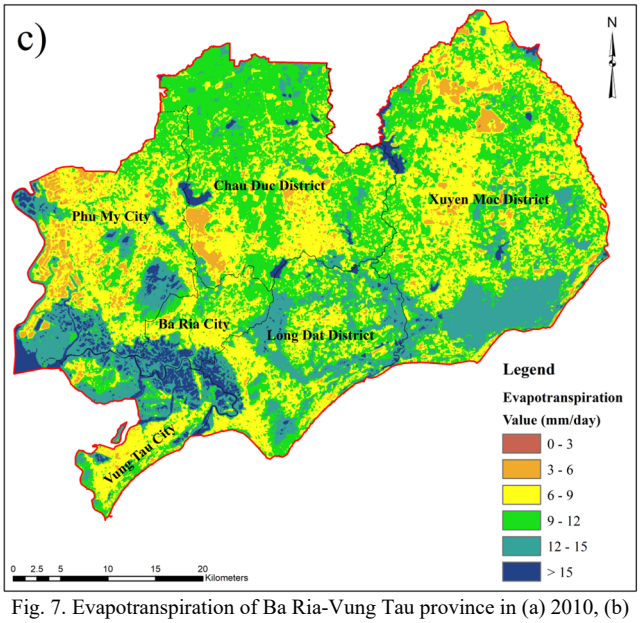

Fig. 7. Evapotranspiration of Ba Ria-Vung Tau province in (a) 2010, (b) 2015, and (c) 2020.

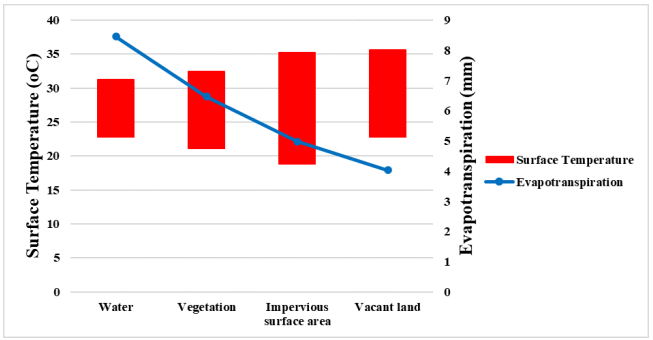

a)

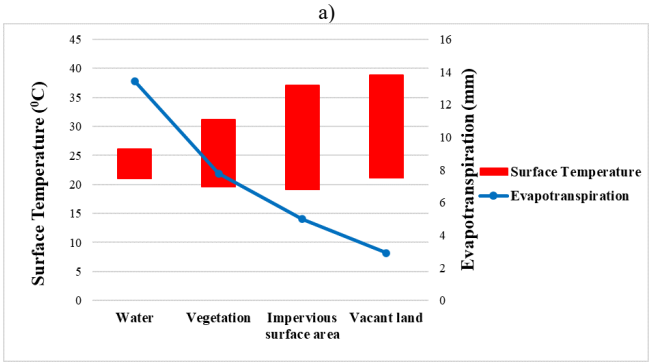

b)

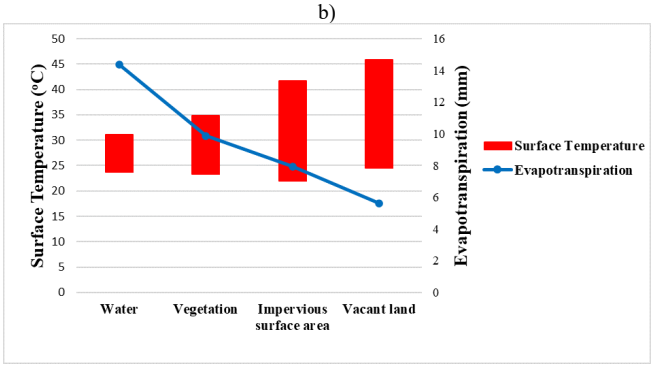

c)

Fig. 8. Surface temperature and evapotranspiration diagram of Ba Ria-Vung Tau province in (a) 2010, (b) 2015, (c) 2020.

IV. Discussion

Results representative of snapshot conditions: In this study, the Landsat satellite images used to estimate Evapotranspiration (ET) included only one image of one day for each year 2010, 2015, and 2020. These images were selected from the dry season (January and February), ensuring low cloud and low surface moisture conditions to clearly reflect the evapotranspiration characteristics of land cover types. However, the ET results obtained from this single-day image only reflect the instantaneous conditions at the time of capture, which is also a drawback because it does not completely represent seasonal or annual ET change. Therefore, the inter-annual variation reflects the spatial variation of ET during the dry season, rather than the continuous variation over time.

Average values: The results show that the average ET value of the water surface reached about 15 mm/day in 2020, calculated from pixels in the water surface layer after classification, which has a strong evaporation capacity in hot and humid tropical conditions, especially in the dry season. In addition, using the S-SEBI model to calculate ET based on the surface energy balance using Landsat images, it is possible to clearly highlight areas such as lakes, rivers, and ponds with high evaporation due to high surface humidity and thermal conductivity, which reflect the surface energy conditions at the time.

Land cover change affects hydrology and ET: the most important variables influencing the geographical magnitude of ET, particularly in areas of rapid urbanization or land use conversion, where vegetation cover is replaced by impervious surfaces or cultivated land [37]. Although climate change is the main factor in large-scale trends of ET change, in areas with strong LULC fluctuations, such as deforestation or conversion to cultivated land, land use change plays a more prominent role in influencing ET [38]. The expansion of built-up and agricultural land has reduced the overall ET value in the region due to the loss of natural vegetation that can retain moisture and regulate water flow [39]. In contrast, areas with high forest cover exhibited higher ET values, indicating the role of vegetation in maintaining the energy and water balance at the surface.

The 7% ET increase from 2010 to 2020, driven by a 1.5°C LST rise, reflects climate warming and land cover shifts in Ba Ria-Vung Tau. Urbanization expanded impervious surfaces by 46.95 km², reducing bare soil by 287.63 km², which lowered ET in urban zones (3–5 mm/day) due to limited water availability. Conversely, water surfaces and vegetation sustained higher ET (15 and 10 mm/day), reinforcing their role as hydrological buffers. This aligns with global patterns—Fisher *et al.* [20] reported ET rates of 65 ± 5 mm/month in humid tropics—and local findings [23, 29, 40], though coastal humidity likely amplifies water surface ET here compared to inland basins.

Hydrologically, elevated ET in vegetated and water-rich areas supports baseflow maintenance, which is critical for dry-season water supply, while low ET in urban zones heightens runoff and water scarcity risks. Annually, this translates to a 5–10% reduction in available water in urban catchments, necessitating enhanced storage solutions—a trend corroborated by Haiyang Shi [22], who found correlation of ET and temperature in drylands and wetlands, based on global data. These maps can guide irrigation allocation, prioritizing natural vegetation to minimize water loss. S-SEBI's reliance on cloud-free imagery may underestimate ET during rainy periods, as Guan *et al.* [21] observed 8–12 mm/day ET in monsoon regions with MODIS, suggesting integration with MODIS for higher temporal resolution to capture seasonal variability more effectively [18].

The S-SEBI ET estimates were validated against the FAO-56 ETp using NASA POWER data at the Vung Tau station. However, this single-point validation does not account for spatial and temporal variability in meteorological conditions across the diverse terrain and land cover of Ba Ria-Vung Tau. NASA POWER data indicate minimal spatial variability in dry season conditions, suggesting that the Vung Tau station is reasonably representative [27]. However, local microclimates, which can lead to ET estimate errors of 10–15%, have been noted by Guan *et al.* (2022) [21]. Future studies should use data from more meteorological stations or reanalysis datasets to capture spatial heterogeneity and improve validation robustness.

The results show that urban heat island activity is very strong, with a decreasing trend from urban to suburban areas. Typical areas with increased surface temperature due to rapid urbanization include Vung Tau city, Ba Ria city, Long Dat

district, and Phu My city. This illustrates that changes in land cover contribute to the area's rising land surface temperature.

Regarding the limitations and future developments of the study, the study makes some specific recommendations to improve the effectiveness of ET estimation and support water resources management in Ba Ria - Vung Tau province [25, 41]. The current study mainly relies on satellite data and modeling due to the lack of data from field monitoring stations. Supplementing information from local monitoring stations is necessary to collect real-time information on surface temperature, air humidity, wind speed, and rainfall. These field data will provide the basis for calibrating and verifying remote sensing models, thereby improving the accuracy of ET estimation. Due to the limitation of research time, the results of the topic are only analyzed in short periods, unable to provide a comprehensive picture of the long-term trend of ET and the impact of climate change. Further long-term studies, continuously monitoring changes in land cover and environmental factors, are needed to predict future trends in climate change and evapotranspiration more accurately. The study should be extended to multiple seasons, especially the dry and wet seasons, or extend the period to compare ET changes better.

V. Conclusions

This study presents the first spatiotemporal Evapotranspiration (ET) dataset for a Vietnamese coastal province, mapping ET across Ba Ria-Vung Tau from 2010 to 2020 using the S-SEBI model and Landsat imagery. Distinct ET variations were observed across land cover types in the province. Water surfaces (15.01 ± 0.5 mm/day) and vegetation (6–10 mm/day) emerged as key hydrological contributors, unlike lower rates in bare soil and impervious surfaces (3–5 mm/day). Land Surface Temperature (LST), which rose by 1.5°C from 27.8°C in 2010 to 29.3°C in 2020, was a key driver of ET, directly influencing its 7% increase over the decade. This rise highlights climate change's impact on coastal water cycles, particularly during the dry season when elevated surface temperatures intensify evaporation. These findings enhance regional water balance understanding and advocate for remote sensing in hydrological planning. We recommend extending this approach to other Southeast Asian coastal regions to optimize water storage and irrigation strategies amid urbanization and warming trends.

Appendix

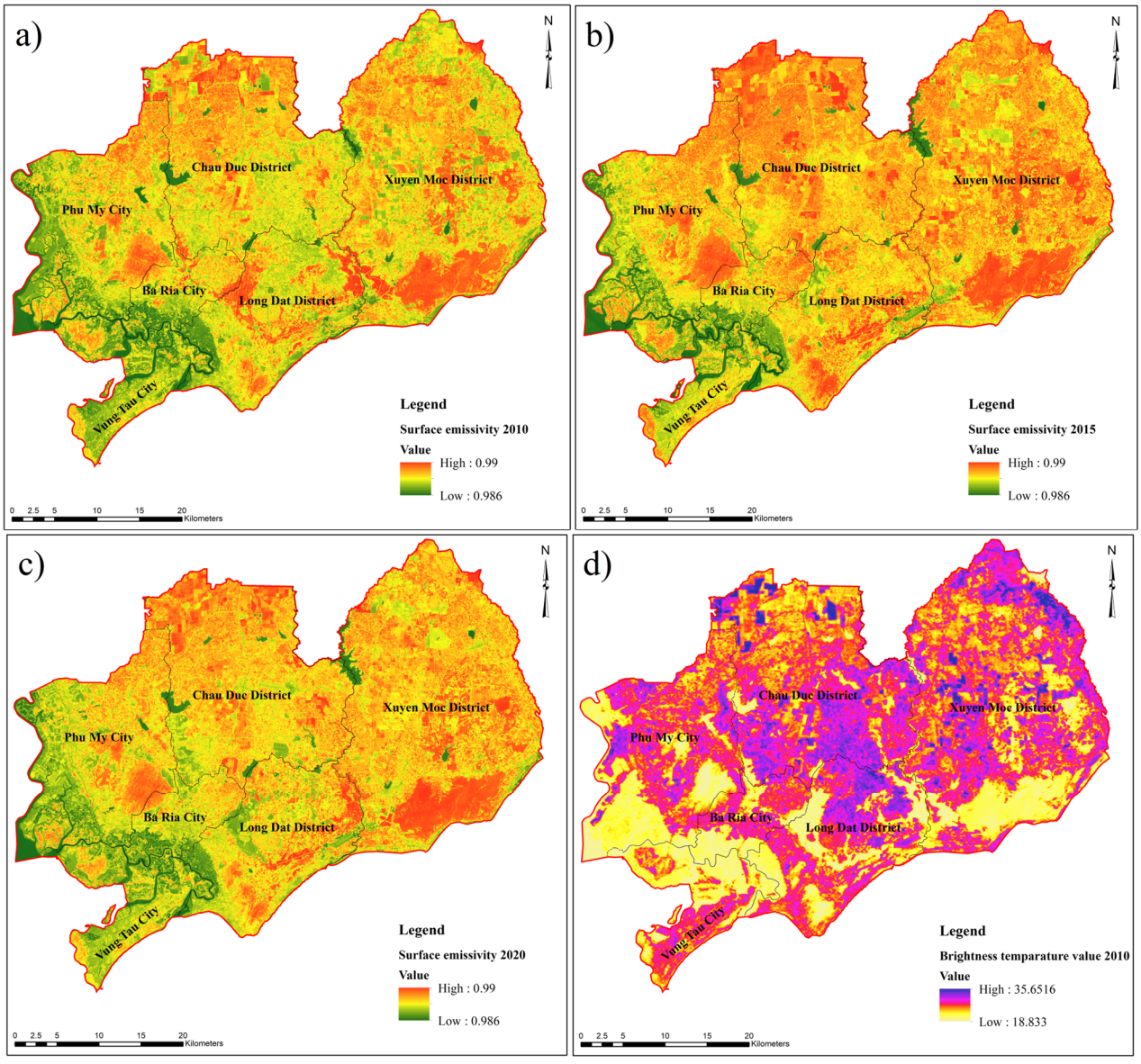

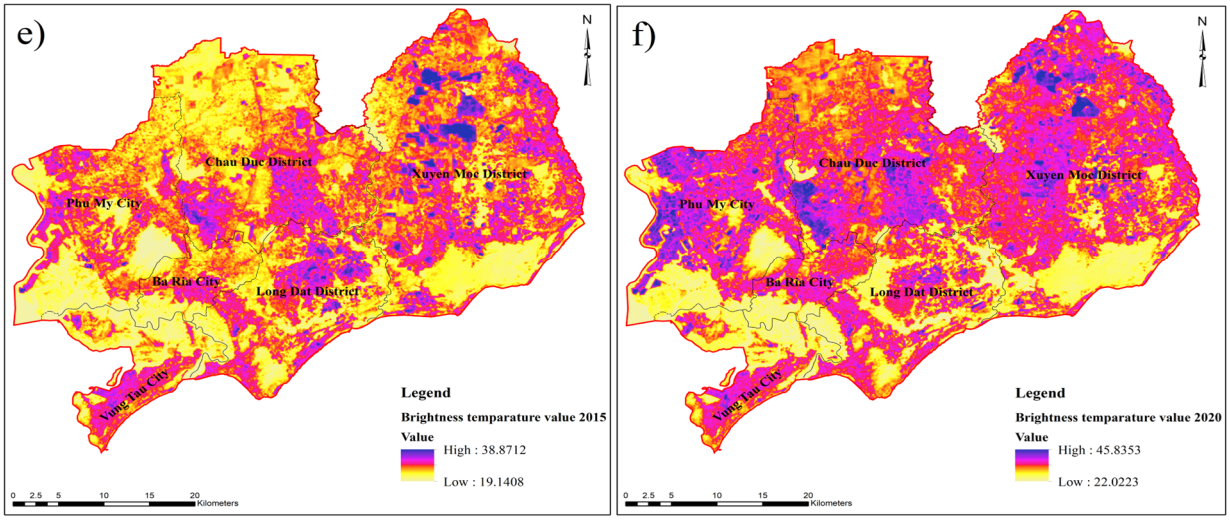

Fig. A1. Results of surface emissivity in (a) 2010, (b) 2015, (c) 2020; and Brightness temperature value in (d) 2010, (e) 2015, (f) 2020.

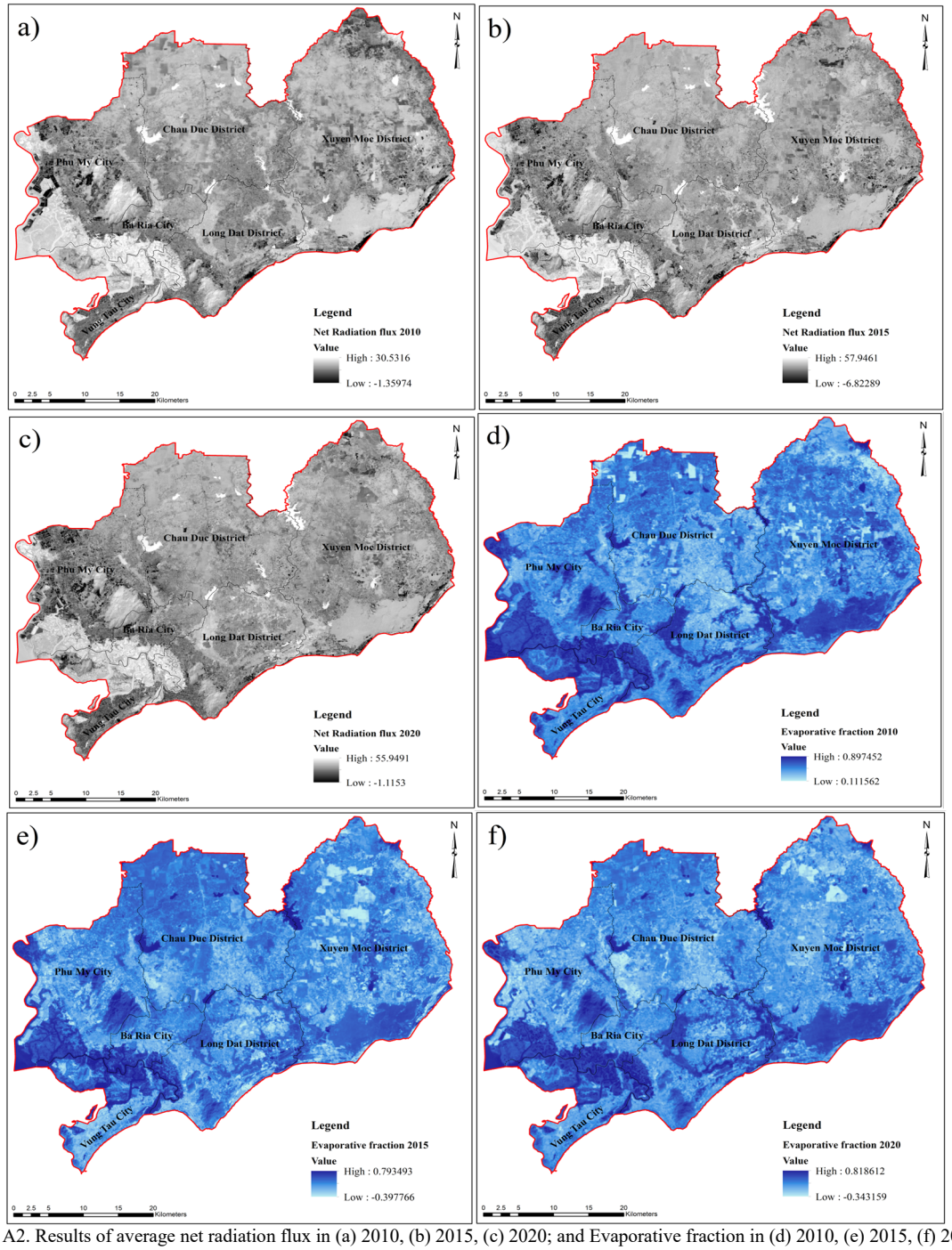

Fig. A2. Results of average net radiation flux in (a) 2010, (b) 2015, (c) 2020; and Evaporative fraction in (d) 2010, (e) 2015, (f) 2020.

Conflict of Interest

The authors declare no conflicts of interest.

Author Contributions

Conceptualization, A.H.N.; methodology, A.H.N. and N.T.T.P.; data collection and analysis, V.M.H.T. and L.K.L.; validation, N.T.T.P; writing—original draft preparation, A.H.N.; writing—review and editing, V.N.Q.K., T.D.N and L.K.L. All authors have read and agreed to the published version of the manuscript. All authors had approved the final version.

Funding

This research is funded by Vietnam National University Ho Chi Minh City (VNU-HCM) under grant number B2025-24-03.

References

[1] R. G. Allen *et al.*. (1998). Crop evapotranspiration—Guidelines for computing crop water requirements. *FAO Irrig. Drain.* [Online]. 56. Available: http://www.climasouth.eu/sites/default/files/FAO%2056.pdf

[2] L. V. Trung. Remote sensing textbook. [Online]. Available: http://lib.hcmunre.edu.vn/Viewer/?ID=2658 (in Vietnamese)

[3] V. L. Nguyen *et al.*, "Assessing the correlation between spectral indices and land surface heat fluxes by remote sensing technology: A case study in Thai Binh Province, Red River Delta, Vietnam," *Remote Sens. Earth Syst. Sci.*, vol. 7, pp. 159–171, 2024.

[4] P. E. Rijtema. (1965). An analysis of actual evapotranspiration. [Online]. Available: https://edepot.wur.nl/315768

[5] J. A. Clark, K. D. Tape, and J. M. Young-Robertson, "Quantifying evapotranspiration from dominant arctic vegetation types using lysimeters," *Ecohydrology*, vol. 16, no. 1, e2484, Jan. 2023.

[6] A. Tahooni, A. A. Kakroodi, and M. Kiavarz, "Monitoring of land surface albedo and its impact on Land Surface Temperature (LST) using time series of remote sensing data," *Ecol. Inform.*, vol. 75, 102118, 2023.

[7] J. Joiner *et al.*, "Global relationships among traditional reflectance vegetation indices (NDVI and NDII), Evapotranspiration (ET), and soil moisture variability on weekly timescales," *Remote Sens. Environ.*, vol. 219, pp. 339–352, 2018.

[8] M. C. Anderso *et al.*, "Interoperability of ECOSTRESS and Landsat for mapping evapotranspiration time series at sub-field scales," *Remote Sens. Environ*., vol. 252, 112189, 2021.

[9] G. H. Hargreaves and Z. A. Samani. (December 1985). Reference crop evapotranspiration from ambient air temperature. [Online]. Available: https://www.researchgate.net/profile/Zohrab-Samani/publication/247373660_Reference_Crop_Evapotranspiration_From_Temperature/links/546e3b620cf2bc99c2155046/Reference-Crop-Evapotranspiration-From-Temperature.pdf

[10] C. H. B. Priestley and R. J. Taylor, "On the assessment of surface heat flux and evaporation using large-scale parameters," *Mon. Wea. Rev.*, vol. 100, pp. 81–92, 1972.

[11] A. Srivastava *et al.*, "Modelling the dynamics of evapotranspiration using variable infiltration capacity model and regionally calibrated Hargreaves approach," *Irrigation Science*, vol. 36, pp. 289–300, 2018.

[12] Y. A. Liou and S. K. Kar, "Evapotranspiration estimation with remote sensing and various surface energy balance algorithms—A review," *Energies*, vol. 7, no. 5, pp. 2821–2849, 2014.

[13] R. Waters *et al.* (August 2002). SEBAL: Surface energy balance algorithms for land: Idaho implementation: Advanced training and users manual. [Online]. Available: https://posmet.ufv.br/wp-content/uploads/2017/04/MET-479-Waters-et-al-SEBAL.pdf

[14] W. J. Timmermans *et al.*, "An intercomparison of the Surface Energy Balance Algorithm For Land (SEBAL) and the Two-Source Energy Balance (TSEB) modeling schemes," *Remote Sens. Environ.*, vol. 108, no. 4, pp. 369–384, 2007.

[15] G. J. Roerink, Z. Su, and M. Menenti, "S-SEBI: A simple remote sensing algorithm to estimate the surface energy balance," *Phys. Chem. Earth, Part B Hydrol. Ocean. Atmos.*, vol. 25, no. 2, pp. 147–157, 2000.

[16] U. Kumar *et al.*, "Evaluation of simplified surface energy balance index (S-SEBI) method for estimating actual evapotranspiration in Kangsabati reservoir command using landsat 8 imagery," *J. Indian Soc. Remote Sens.*, vol. 48, pp. 1421–1432, 2020.

[17] C. Mattar *et al.*, "Impacts of the broadband albedo on actual evapotranspiration estimated by S-SEBI model over an agricultural area," *Remote Sens. Environ.*, vol. 147, pp. 23–42, 2014.

[18] J. K. Kiptala *et al.*, "Mapping evapotranspiration trends using MODIS and SEBAL model in a data scarce and heterogeneous landscape in Eastern Africa," *Water Resources Research*, vol. 49, no. 12, pp. 8495-8510, 2013.

[19] A. Rajeshwari and N. Mani, "Estimation of land surface temperature of Dindigul district using landsat 8 data," *Int. J. Res. Eng. Technol.*, vol. 3, no. 5, pp. 122–126, 2014.

[20] R. K. Vinukollu *et al.*, "Global estimates of evapotranspiration for climate studies using multi-sensor remote sensing data: Evaluation of three process-based approaches," *Remote Sens. Environ.*, vol. 115, no. 3, pp. 801–823, 2011.

[21] X.Guan *et al.*, "Integrating MODIS and Landsat data for land cover classification by multilevel decision rule," *Land*, vol. 10, no. 2, 208, 2021.

[22] H. Shi, "Evapotranspiration trends over the last 300 years reconstructed from historical weather station observations via machine learning," arXiv Preprint, arXiv: 2407.16265, 2024. doi: 10.48550/arXiv.2407.16265

[23] N. V. Hung, "Determination of actual evapotranspiration in the Cau River Basin using Landsat imagery," *Journal of Geodesy and Cartography*, vol. 30, pp. 42–49, 2016. (in Vietnamese)

[24] T. Van Kich *et al.*, "Building high-resolution evapotranspiration maps for Soc Trang province from sentinel remote sensing images," *Vietnam Journal of Hydrometeorology*, vol. 741, pp. 1–10, 2022. (in Vietnamese)

[25] A. H. Nguyen, V. M. Hong Tat, and T. T. T. Hoang, "Assessing groundwater vulnerability and addressing salinization in the coastal region of Ba Ria-Vung Tau province, Vietnam: An enhanced DRASTIC model approach," *Environ. Earth Sci.*, vol. 83, 53, 2024.

[26] General Statistics Office. (June 2023). Statistical yearbook of Viet Nam 2022. [Online]. Available: https://www.nso.gov.vn/en/data-and-statistics/2023/06/statistical-yearbook-of-2022/

[27] G. C. Rodrigues and R. P. Braga, "Estimation of daily reference evapotranspiration from NASA POWER reanalysis products in a hot summer mediterranean climate," *Agronomy*, vol. 11, no. 10, 2077, 2021.

[28] A. M. G. Faramiñán *et al.* "Estimation of actual evapotranspiration using NASA-POWER data and support vector machine," in *Proc. 2021 XIX Workshop on Information Processing and Control (RPIC)*, 2021, pp. 1–5.

[29] L. H. Chien, "Study on developing a model for monitoring evapotranspiration of land cover in northwest Vietnam using satellite imagery," Ph.D. dissertation, Dept. Surveying and Mapping Engineering, University of Mining and Geology, Hanoi, Vietnam, 2022. https://humg.edu.vn/content/tintuc/Lists/News/Attachments/8238/Toan%20van%20luan%20an.pdf (in Vietnamese)

[30] J. A. Richards and X. Jia, "The Interpretation of Digital Image Data," in *Remote Sensing Digital Image Analysis*, Heidelberg: Springer, 1999, ch. 1, pp. 75–88.

[31] J. A. Richards, X. Jia, "Error Correction and Registration of Image Data," in *Remote Sensing Digital Image Analysis*, Heidelberg: Springer, 1999, ch. 1, pp. 39–74.

[32] N. T. Can *et al.*, "Analysis of factors influencing the surface urban heat island phenomenon in the Bangkok metropolitan area, Thailand," *J. Sci. VNU Earth Environ. Sci.*, vol. 35, no. 1, pp. 53–62, 2019. (in Vietnamese)

[33] M. Shahzaman *et al.* "Remote sensing indices for spatial monitoring of agricultural drought in South Asian countries," *Remote Sensing*, vol. 13, no. 20, 2059, 2021.

[34] N. Kumari, A. Srivastava, and U. C. Dumka, "A long-term spatiotemporal analysis of vegetation greenness over the Himalayan region using google earth engine," *Climate*, vol. 9, no. 7, 109, 2021.

[35] D. Chicco, M. J. Warrens, and G. Jurman, "The coefficient of determination R-squared is more informative than SMAPE, MAE, MAPE, MSE and RMSE in regression analysis evaluation," *Peerj Comput. Sci.*, vol. 7, e623, 2021.

[36] N. V. Hung, "Application of remote sensing data to determine solar radiation-induced evaporation in the Cau River Basin," Ph.D. dissertation, Dept. Surveying and Mapping Engineering, Institute of Surveying and Mapping Science, Hanoi, Vietnam, 2017. https://media.visam.vn/wwwroot/documents/LUAN%20AN%20TS%20NGUYEN%20V%C4%82N%20HUNG_1663645730220.pdf (in Vietnamese)

[37] C. B. Pande *et al.*, "Impact of land use/land cover changes on evapotranspiration and model accuracy using google earth engine and classification and regression tree modeling," *Geomatics, Natural Hazards and Risk*, vol. 15, no. 1, 2290350, 2024.

[38] G. Li *et al.* "Response of evapotranspiration to changes in land use and land cover and climate in China during 2001–2013," *Science of the Total Environment*, vol. 596, pp. 256–265, 2017.
[39] R. K. Bhardwaj, S. Sharma, and D. Kumar, "Impact of LULC dynamics on evapotranspiration using GIS: Case study of Uttarakhand," *J. Mater. Environ. Sci*., vol. 13, no. 6, pp. 631–639, 2022.
[40] H. C. Le, "Determining the linear coefficient of the Priestley-Taylor model for estimating evapotranspiration in Hoa Binh province, Northwest Vietnam," *Journal of Geodesy and Cartopraphy*, vol. 50, pp. 46–56, 2022. (in Vietnamese)
[41] P. T. Ha *et al.* "Quantitative exploration of the innovative trend method for evapotranspiration and its sensitivity to climatic variables: The case study of Southeast Vietnam," *Earth Sci. Informatics*, vol. 17, pp. 299–314, 2024.